Supported iron-based catalysts under influence of static magnetic field for the removal of TBP and EDTA

Ritu D. Ambashta[a], Amit Bhatnagar[b], Mika E.T. Sillanpää[c],*

[a]Backend Technology Development Division, Bhabha Atomic Research Centre, Trombay, Mumbai 400085, India
[b]Faculty of Health and Life Sciences, Department of Biology and Environmental Science, Linnaeus University, Kalmar SE-391 82, Sweden
[c]Laboratory of Green Chemistry, Faculty of Technology, Lappeenranta University of Technology, Sammonkatu 12, Mikkeli FI-50130, Finland, Tel. +358 400 205 215; email: Mika.Sillanpaa@lut.fi

ABSTRACT

Zerovalent metals offer decontamination of organic toxins in aqueous medium. In the present study, alumina-based iron and iron–nickel in the presence and the absence of magnetic field for the decontamination of tributyl phosphate (TBP) and ethylene diamine tetraacetic acid (EDTA) has been compared. TBP decontamination was improved in the presence of zerovalent metals. EDTA decontamination was not enhanced in the presence of zerovalent metals. The decontamination of TBP using iron-based alumina was higher than iron–nickel. The surface interaction on alumina surface, as characterized by attentuated total reflectance-Fourier transform infrared spectroscopy, and the surface interaction on metallic elements, as characterized by evaluating the magnetic moment values helped to understand the reason for the difference in role of alumina-based iron and iron–nickel on decontamination of TBP and EDTA.

Keywords: Magnetic nanocatalyst; Degradation; TBP; EDTA; SQUID magnetization

1. Introduction

The scale of groundwater contamination is enormous owing to the limited regulatory practices of industrial and agricultural sources. Two groundwater pollutants considered in this regard are tributyl phosphate (TBP) and ethylene diamine tetraacetic acid (EDTA). TBP finds application as flame retardants, plasticizers, and solvents; and being carcinogenic, its discharge needs to be controlled [1–3]. EDTA is a common complexing agent and used in many industrial applications [4–11]. Although nontoxic by itself, it forms stable complexes with heavy metals that are toxic and therefore, its discharge also needs to be controlled [12–14]. The nuclear industry employs both TBP and EDTA extensively; therefore, this study has more significant relevance to the industry [15]. In recent decades, the potential of iron metal for aquatic contaminants removal has been widely studied and has shown encouraging results in water treatment especially organics degradation [16,17]. The corrosion reaction using bimetallic or zero-valent iron has been exploited for the degradation of several organics [18,19]. With the advancement of nanotechnology, it was proposed that nanoscale iron degrades organic pollutants at a far superior rate than the granulated

*Corresponding author.

ones [20]. Furthermore, it has been found in several studies that nickel aides in enhancing the corrosion of iron and extensive studies have been reported for iron–nickel for the degradation of organics [21–25].

Magnetic material-supported catalysts have been reported to be advantageous for improvising the efficiency of catalyst [26,27]. It is known that iron and nickel are strong ferromagnets. It has therefore been argued that the catalysts should not be employed under magnetic field since owing to their aggregation; this would result in loss of reactivity [16]. However, when synthesized on support matrix, they would not aggregate under influence of magnetic field due to polar interactions, van der Waals interactions, and steric hindrance. In addition, the presence of magnetic field can significantly influence the redox behavior of iron-based catalysts. Several researchers have prepared magnetic metals and alloys on alumina, however, their catalytic properties under the influence of magnetic field has not been exploited [28–33].

In the present study, iron and iron–nickel powders supported on alumina are investigated to evaluate the decontamination behavior of TBP and EDTA. A comparison of the degradation under magnetic field influence is also presented to analyze the difference in release of ions from catalyst during redox reactions of the catalyst.

2. Experiments

2.1. Materials and methods

Chromatographic grade alumina (M/s Fluka) in the size range 15–150 μm was used as support matrix. Analytical grade sodium borohydride (M/s Sigma Aldrich), iron (II) chloride (M/s Fluka), nickel (II) nitrate, and palladium (II) chloride (M/s Sigma-Aldrich) were used for the catalyst preparations. Analytical grade TBP (M/s Sigma Aldrich) and EDTA (M/s Sigma Aldrich) were used as surrogates for organic pollutants.

2.2. Catalyst preparation

The catalysts were prepared by loading iron and iron–nickel, respectively, on alumina substrate. The ratio of sodium borohyride to metal was 1.2:1 by weight. The iron: nickel ratio was 1:1 for iron–nickel-based catalyst. The metal salt was taken in solution and added to mixture of alumina powder and sodium borohydride. This mixture was continuously stirred until gas evolution ceased and then loaded to a glass column (7.5 mm ID × 250 mm D). Washing was followed with pH 4 HCl for about four times. The

alumina powder in batches of 0.5 g was loaded with 1% catalyst by this method.

2.3. Column studies experiment setup

The solubility of TBP is 400 mg/L and that of ETDA is 500 mg/L in water at 25℃. In order to be within solubility limits, 300 mg/L of both TBP and EDTA was prepared for the experiments. The applicability of the zero-valent iron in low pH ranges for organic destruction has been cited [16]. We have used pH 4 for our studies. Stock solutions of 300 mg/L TBP and 300 mg/L Na_2H_2EDTA were prepared in pH 4 HCl. Direct current powered electromagnet procured from M/s SVS Lab Inc was used in the experiments. Feed solution of TBP and EDTA were allowed to flow through column at a rate of 1 mL/min both in presence and absence of magnetic field. The effluent was directly analyzed for total organic content and metal impurity.

2.4. Characterization of materials

PANalytical X'Pert Pro MPD-model XRD was used to study the crystalline nature of the powders. The step size was kept at ~0.1^0 for each measurement duration around 2 h 45 min. Hitachi S-4800 Ultra-High Resolution Scanning Electron Microscope (SEM) was used to understand the morphology of powders. Nicolet 4700 Fourier transform infrared spectroscopy (FTIR) was used in attentuated total reflectance (ATR) mode to obtain the infrared spectra on powder samples. Deuterated triglycine sulfate CsI detector was used in the measurements. For each sample, the resolution of the scans was kept at 4 cm^{-1}, the number of sample scans was 16 and each sample scan was preceded by a background scan. The magnetization data was collected on Quantum design make SQUID-MPMS XL. Each sample of ~10 mg weight was sealed in a Teflon tape and tightly encapsulated in a gelatine capsule. The capsule was placed at center of gelatin straw for the measurements. The total organic carbon (TOC) analysis was carried out using TOC-VCPH Shimadzu Analyzer. Freshly prepared TOC standards were used for calibration of unit. This was followed by direct measurements on column effluent samples.

3. Results and discussion

3.1. X-ray diffraction pattern

The X-ray diffraction (XRD) pattern of the samples is shown in Fig. 1. The data suggests that on account of the amorphous nature of the metal nanoparticles, it is difficult to identify them with respect to alumina.
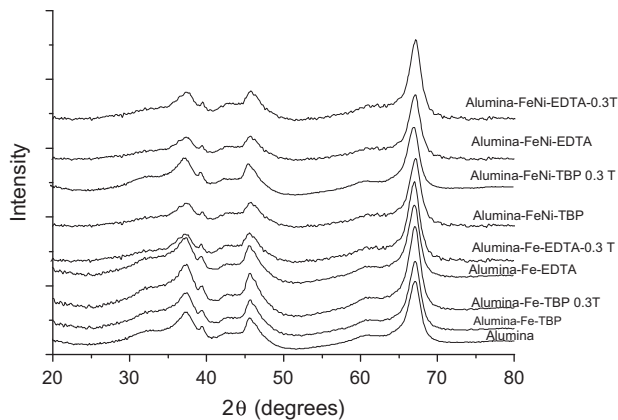
Fig. 1. XRD pattern of samples.

3.2. SEM data

A typical alumina particle of ~20 μm is shown in Fig. 2. Focusing on the surface of catalyst-loaded alumina shows a flake-like morphology of the catalyst. This morphology is suggestive of nanopowder formation. There was no difference in morphology of iron- and iron–nickel-loaded samples.
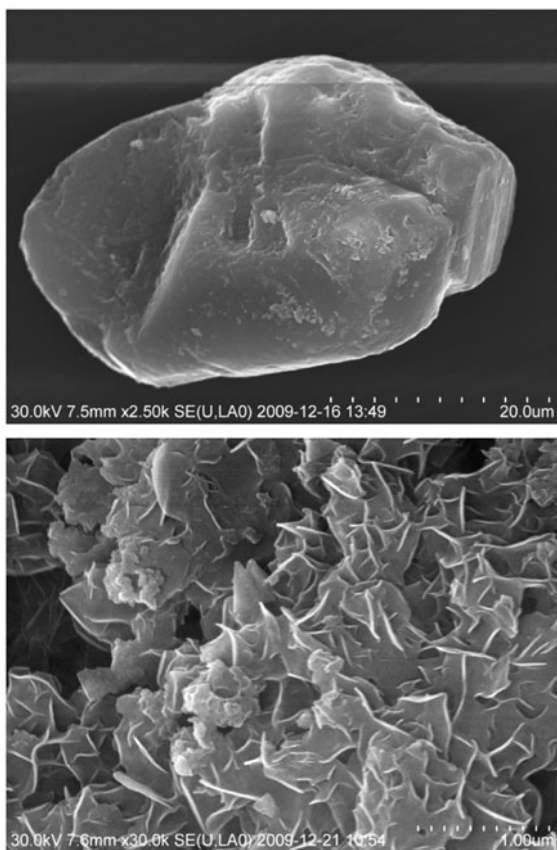

Fig. 2. SEM image of alumina and catalyst loaded alumina.

3.3. TOC analyses and TBP and EDTA removal

The removal efficiency of the organic compounds was analyzed using TOC analyzer. The standard deviation calculated using the TOC standards was about 4% in the measurements. The ratio of initial and final carbon with time was evaluated for TBP and EDTA-interacted samples in presence and absence of magnetic field. The chromatographic grade alumina in the absence of catalyst removes TBP to 59% and EDTA to 45% suggesting that alumina is capable of sorbing the solvents onto its surface.

The plot of initial carbon to final carbon for interactions with iron-based catalyst on alumina interacted with 300 ppm TBP/EDTA at pH 4 is shown in Fig. 3(a). On addition of iron-based catalyst, the
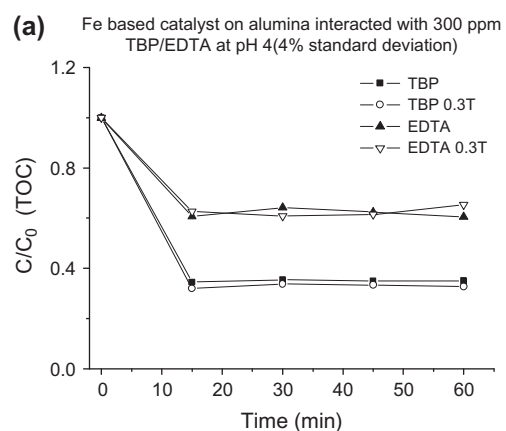

Fig. 3a. Plot of carbon ratios (TOC) vs. time for iron-based alumina interacted with TBP and EDTA in presence and absence of magnetic field.
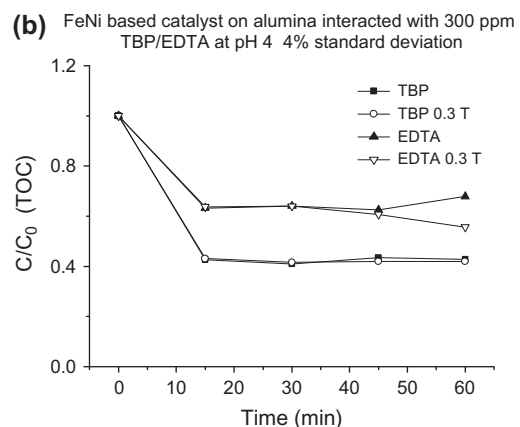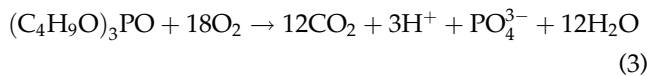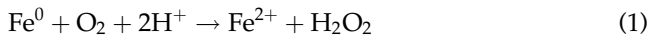

Fig. 3b. Plot of carbon ratios (TOC) vs. time for iron–nickel-based alumina interacted with TBP and EDTA in presence and absence of magnetic field.
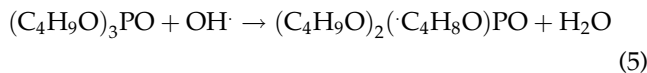
removal was found to be more than 65% in case of TBP. On the other hand, the removal was reduced to 40% in case of EDTA. In the presence of magnetic field, the removal of TBP was slightly improved but EDTA removal remained unaffected.

The plot of initial carbon to final carbon for interactions with Fe–Ni-based catalyst on alumina interacted with 300 ppm TBP/EDTA at pH 4 is shown in Fig. 3(b). On addition of iron–nickel-based catalyst, EDTA removal does not differ from iron but the TBP removal was rendered more sluggish with 59% removal of TBP. This removal efficiency was same as for non catalyst loaded alumina. The behavior in presence and in the absence of field does not differ.

The decontamination of TBP and EDTA has been proposed through oxidative transformation of iron [18,34,35]. Iron degrades TBP according to the mechanism shown below (Eq. (1)–(5)),
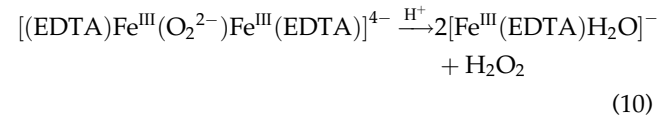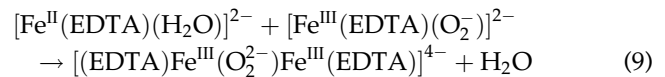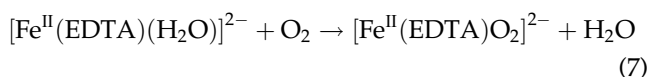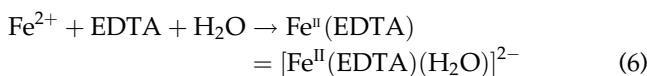
$$Fe^0 + O_2 + 2H^+ \rightarrow Fe^{2+} + H_2O_2 \tag{1}$$

$$H_2O_2 \rightarrow H_2O + \frac{1}{2}O_2 \tag{2}$$

$$(C_4H_9O)_3PO + 18O_2 \rightarrow 12CO_2 + 3H^+ + PO_4^{3-} + 12H_2O \tag{3}$$

Alternatively,

$$Fe^{2+} + H_2O_2 \rightarrow FeOH^{2+} + OH^{\cdot} \tag{4}$$

$$(C_4H_9O)_3PO + OH^{\cdot} \rightarrow (C_4H_9O)_2(^{\cdot}C_4H_8O)PO + H_2O \tag{5}$$

The radical after multi-stages degrades to the mineralized forms of equation (3).

In the presence of oxygen, EDTA reduced the presence of accumulated Fe^{2+} near the zero-valent iron surface and thus, prevented scavenging of hydroxyl radicals by Fe^{2+} or facilitated a modified Fenton process in solution. It also aided in the enhancement of H_2O_2 production [36–38].

$$Fe^{2+} + EDTA + H_2O \rightarrow Fe^{II}(EDTA)$$
$$= [Fe^{II}(EDTA)(H_2O)]^{2-} \tag{6}$$

$$[Fe^{II}(EDTA)(H_2O)]^{2-} + O_2 \rightarrow [Fe^{II}(EDTA)O_2]^{2-} + H_2O \tag{7}$$

$$[Fe^{II}(EDTA)O_2]^{2-} \rightarrow [Fe^{III}(EDTA)O_2^-]^{2-} \tag{8}$$

$$[Fe^{II}(EDTA)(H_2O)]^{2-} + [Fe^{III}(EDTA)(O_2^-)]^{2-}$$
$$\rightarrow [(EDTA)Fe^{III}(O_2^{2-})Fe^{III}(EDTA)]^{4-} + H_2O \tag{9}$$

$$[(EDTA)Fe^{III}(O_2^{2-})Fe^{III}(EDTA)]^{4-} \xrightarrow{H^+} 2[Fe^{III}(EDTA)H_2O]^- + H_2O_2 \tag{10}$$

$$Fe^{II}EDTA + H_2O_2 \rightarrow Fe^{III}EDTA + OH^- + OH^{\cdot} \tag{11}$$

No decomposition reaction of EDTA took place using iron catalyst or iron–nickel catalyst. It has been reported that the oxidation of iron can be enhanced by using a more electropositive ion nickel [39–41]. In the present study however, it was observed that the bimetallic did not aide in enhancing degradation of TBP or EDTA. It has been reported that the pathway of zerovalent iron for degradation of organics takes place via direct electron transfer process from metal surface; corrosion of metal or reduction of organic through galvanic cell formation on surface of metal. In case of degradation of TBP and EDTA, oxidative transformation was required. The presence of nickel had passivated the surface of iron and therefore did not allow enhancement of oxidation of iron. EDTA removal from the TOC data appeared primarily through the adsorption on alumina surface and formation of soluble complex of oxidized catalyst.

The TOC data could be fitted to second-order kinetic model according to Eq. (12).

$$t/C = 1/(k_2C_0^2) + t/C_0 \tag{12}$$

where C_0 is initial amount of carbon and C is amount of carbon after time t. K_2 is the rate constant in units $mg\,L^{-1}\,min^{-1}$. The rate constants are summarized in Table 1.

Table 1
Rate constant from second-order fitted model for different samples

Sample	K_2 (mgL^{-1} min^{-1})
Alumina-Fe-EDTA	−2.73
Alumina-Fe-EDTA-0.3 T	1.41
Alumina-FeNi-EDTA	1.27
Alumina-FeNi-EDTA-0.3 T	−0.64
Alumina-Fe-TBP	33.83
Alumina-Fe-TBP-0.3 T	−21.82
Alumina-FeNi-TBP	3.71
Alumina-FeNi-TBP-0.3 T	−10.44

3.4. Inductively coupled plasma analyses

The concentration of Fe and Ni in samples of effluent after column run is shown in Table 2. The loss of ions to solution in the case of EDTA-interacted samples was more than in the case of TBP-interacted samples. The loss of ions was lower in presence of magnetic field than in absence of magnetic field. The mechanism of EDTA and TBP shown above justifies the higher amount of metal ion for EDTA than TBP.

3.5. ATR-FTIR analyses

There is evidently a large variation in the spectra from one sample to another suggesting that the mechanism of interaction differs for the samples. The region 1,100–300 cm^{-1} is prominent characteristic of Al–O vibrations in symmetric or asymmetric mode [42–44]. With respect to alumina, the change in these bands on interaction with iron-based samples is shown in Fig. 4 and iron–nickel-based samples is shown in Fig. 5. The absorption bands with minima at 1,057 cm^{-1} are characteristic of symmetric O–Al–O vibrations. The bands with minima at 836 and 738 cm^{-1} are characteristic of asymmetric O–Al–O stretch. In case of iron-based alumina interacted with TBP in the absence of magnetic field, the minima of 1,057 cm^{-1} moves to higher wave number 1,063 cm^{-1}, while the symmetric bands merges with a minima at 811 cm^{-1}. The change in spectra with respect to alumina suggested that degradation reaction on alumina surface affected the symmetric vibration bands more strongly. When TBP interacted with iron-based alumina at a magnetic field of 0.3 T, the asymmetric

Table 2
Amount of iron and nickel in solution analyzed after interaction with different organics in presence and absence of magnetic field

Sample	Concentration in solution (ppm)	
	Fe	Ni
Alumina-Fe-EDTA	82.2	–
Alumina-Fe-EDTA-0.3 T	73	–
Alumina-FeNi-EDTA	55.6	28.4
Alumina-FeNi-EDTA-0.3 T	36	26.2
Alumina-Fe-TBP	2.16	–
Alumina-Fe-TBP-0.3 T	2.14	–
Alumina-FeNi-TBP	0.48	0.56
Alumina-FeNi-TBP-0.3 T	0.38	0.44

Note: The element nickel was not present in the samples and therefore was not analyzed.

stretch band completely merges with the symmetric band forming a broad band with minima fixed at 811 cm^{-1} as above. In presence of magnetic field, the removal of TBP was marginally improved. The surface of alumina was activated by oxidation reactions of iron affecting both the asymmetric and symmetric vibrations of alumina.

In case of iron-based alumina interacted with EDTA in the absence of magnetic field, the 1,057 cm^{-1} band disappears and the symmetric stretch bands merge with minima at 817 cm^{-1}. There is a broad band in the 1,600 cm^{-1} range corresponding to adsorbed water molecule. The bands with minima at 1,012, 1,142, and 1,314 cm^{-1} are corresponding to vibration bands in EDTA [45]. EDTA is more polar as compared to TBP leading to strong adsorption on the surface of alumina; therefore prominent signal of EDTA is observed. When EDTA interacted in the presence of magnetic field the symmetric band of alumina broadened with minima shifted to 800 cm^{-1}. The adsorbed water molecule in presence of magnetic field reacted with the surface of alumina to form aluminum hydroxide. The wave number 1,150, 1,020, 1,379, and 1,461 cm^{-1} is characteristic of aluminum hydroxide and is present in the broadened spectra [46]. The EDTA bands also broadened with lowered intensity as compared to interacted sample in absence of field. It has been reported that EDTA forms insoluble iron EDTA solid compounds. The line broadening of EDTA could be accounted to formation of this compound [18].

The interaction of iron–nickel-based catalyst with TBP and EDTA in presence and absence of magnetic field is presented in Fig. 5. In case of iron–nickel-based alumina samples interacted with TBP, the symmetric bands of alumina merged with minima at 811 cm^{-1}. The asymmetric stretch band at 1,057 cm^{-1} remained unchanged. In the presence of magnetic field, band at 1,124, 1,063, 1,026, and 1,000 cm^{-1} corresponding to aluminum hydroxide appear. The maxima of 1,057 cm^{-1} band disappear. The data suggest that iron–nickel stayed passivated in presence of magnetic field, but the alumina surface under influence of magnetic field interacted with hydrated molecules and formed hydroxyl bonded surface.

In case of iron–nickel-based alumina samples interacted with EDTA, the symmetric bands merge with minima at 806 cm^{-1}. The asymmetric band at 1,057 cm^{-1} disappeared. The bands of EDTA and aluminum hydroxide merged with minima at 1,111 and 1,008 cm^{-1}. In case of EDTA-interacted samples in the presence of magnetic field of 0.3 T, the symmetric bands are merged with minima at 800 cm^{-1}. The bands at
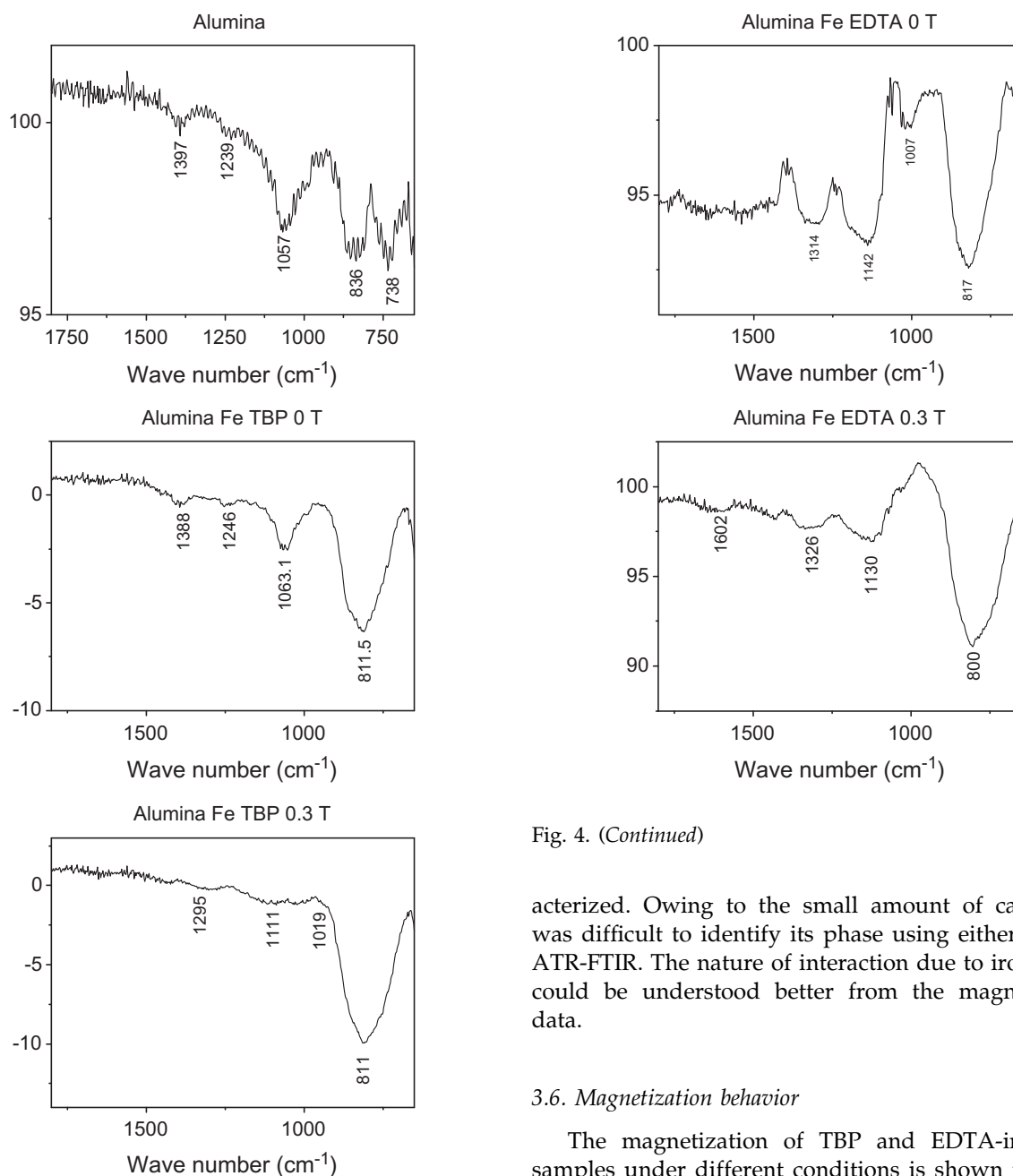
Fig. 4. ATR-FTIR spectra of alumina, iron-based alumina interacted with TBP in absence of magnetic field, iron-based alumina interacted with TBP at 0.3 T, Iron-based alumina interacted with EDTA in absence of magnetic field, and iron-based alumina interacted with EDTA at 0.3 T.

1,130, 1,065, and 1,027 cm^{-1} characteristic of aluminum hydroxide were observed.

The ATR-FTIR bands of iron oxide or iron–nickel oxide, if present, were masked in the symmetric bands of alumina and therefore could not be separately char-

Fig. 4. (*Continued*)

acterized. Owing to the small amount of catalyst, it was difficult to identify its phase using either XRD or ATR-FTIR. The nature of interaction due to iron–nickel could be understood better from the magnetization data.

3.6. Magnetization behavior

The magnetization of TBP and EDTA-interacted samples under different conditions is shown in Fig. 6. The diamagnetic component from the data was subtracted and only the ferromagnetic component in first quadrant is presented in Fig. 6. Although, alumina is diamagnetic and also EDTA and TBP are non-contributors to the actual moment in the sample, their presence influenced the magnetization behavior of the catalyst due to various interactions involved in the presence of atmospheric oxygen. The magnetization data suggested that catalysts interacted in presence of magnetic field possessed higher magnetic moment than the catalysts interacted in the absence of magnetic field. The electron transfer changed the local
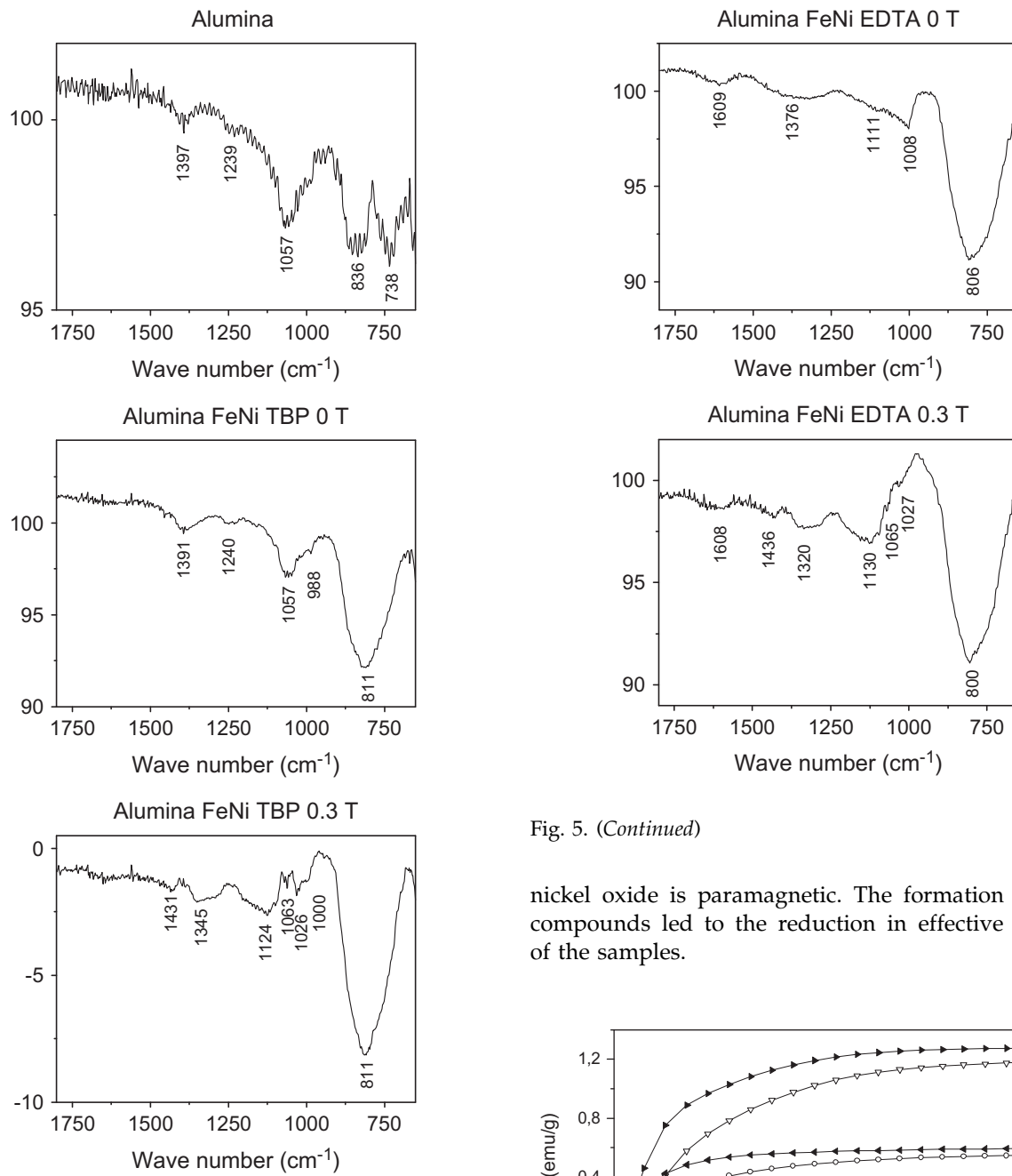
Fig. 5. (*Continued*)

Fig. 5. ATR-FTIR pattern of alumina, iron and iron–nickel-based alumina.

nickel oxide is paramagnetic. The formation of these compounds led to the reduction in effective moment of the samples.

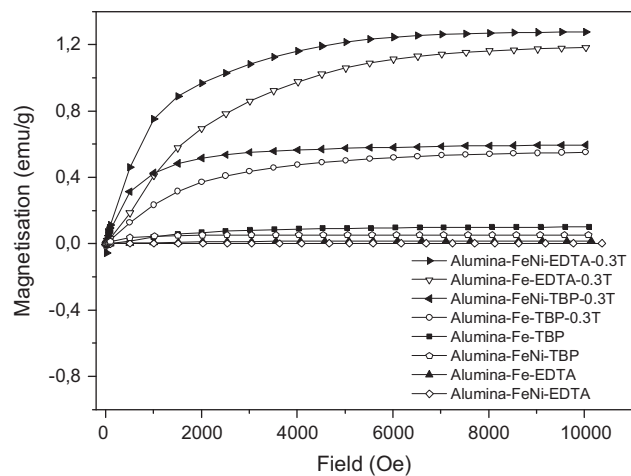Fig. 6. Magnetic moment vs. magnetic field for iron and iron–nickel-based alumina.

electromagnetic field around catalyst atom leading to a significant variation in magnetic moment. The presence and absence of field therefore, contributed to a large variation in magnetic moment of the samples [29,32,47]. Iron and nickel are ferromagnetic while the properties of their oxides differ. Mixed-valent iron oxide or iron–nickel oxide is ferromagnetic while

When EDTA was interacted in presence of magnetic field, the moment of sample was observed as higher than for TBP. The TOC data suggested that EDTA did not decompose catalytically. Iron–Nickel in oxidized form complexed to EDTA and released ions to solution and the remaining fraction on sample was therefore unreacted iron–nickel in metallic state and therefore carried high moment. TBP interactions were catalytic therefore mixed oxidation state compound formation lead to lowering of moments of samples. In addition, in presence of magnetic field, the transformation to low magnetic state compound was rendered sluggish. This also contributed to the higher moment of samples interacted in the presence of magnetic field.

In absence of magnetic field, the magnetization of iron–nickel-based catalyst interacted with EDTA was least, followed by iron–nickel interacted with TBP; EDTA interacted iron and finally iron-interacted TBP. EDTA formed metal complexes in variable oxidation states. The lowering of magnetization suggested that corrosion of catalyst was extensive in presence of EDTA; more in case of iron–nickel than iron-based catalyst. This followed the reason for least moment of EDTA-interacted iron–nickel-based samples.

Although metal ion concentration in solution was high in case of EDTA than TBP, both in the presence and the absence of magnetic field, the magnetization value was more affected with variation in oxidation state than loss of ions to solution. From the moment values of the samples, it was evident that more variable oxidation state is present in absence of magnetic field than in presence of magnetic field.

Different oxidation methods have demonstrated the degradation of TBP to the extent of 100% using photooxidation or chemical oxidation methods [18,48,49]. The extent of degradation is lower in the present study due to low loading of catalyst to alumina. In case of photooxidation or chemical oxidation, there will be toxicity release to the environment. The lower release of ions in presence of magnetic field suggests that the present study provides a more environment-friendly technology for degradation.

In case of EDTA, catalytic wet oxidation technique with supported iron removed 1 mM EDTA to the extent of 40% but the reaction time for the removal was 5 h [50]. In the present study, the time for removal of EDTA is smaller. Although the extent of degradation was low in the present study, in presence of magnetic field, the magnetization and infrared data suggested that degraded EDTA in the form of insoluble iron compound could be retained on alumina so iron release was lowered.

4. Conclusions

The supported catalyst in presence of magnetic field loose lesser ions to solution than in absence of magnetic field. The TBP removal efficiency is enhanced in presence of iron-based catalyst. The iron–nickel-based catalyst do not serve advantageous for removal of either TBP or EDTA. EDTA removal is lowered in the presence of either catalyst iron or iron–nickel suggesting that oxidative decomposition could not be carried out for EDTA under the conditions applied. ATR-FTIR suggests that alumina surface characteristics significantly change in the presence of catalyst in presence and absence of magnetic field. The magnetization data also suggest that presence and absence of field alters the nature of interactions significantly.

Acknowledgment

References

[1] A. Bacaloni, F. Cucci, C. Guarino, M. Nazzari, R. Samperi, A. Laganà, Occurrence of organophosphorus flame retardant and plasticizers in three volcanic lakes of central Italy, Environ. Sci. Technol. 42 (2008) 1898–1903.

[2] A. Marklund, B. Andersson, P. Haglund, Organophosphorus flame retardants and plasticizers in Swedish sewage treatment plants, Environ. Sci. Technol. 39 (2005) 7423–7429.

[3] E. Fries, W. Püttmann, Monitoring of the three organophosphate esters TBP, TCEP and TBEP in river water and ground water (Oder, Germany), J. Environ. Monit. 5 (2003) 346–352.

[4] B. Eklund, E. Bruno, G. Lithner, H. Borg, Use of ethylenediaminetetraacetic acid in pulp mills and effects on metal mobility and primary production, Environ. Toxicol. Chem. 21 (2002) 1040–1051.

[5] B. Nowack, Environmental chemistry of aminopolycarboxylate chelating agents, Environ. Sci. Technol. 36 (2002) 4009–4016.

[6] M. Sillanpää, M. Orama, J. Rämö, A. Oikari, The importance of ligand speciation in environmental research: A case study, Sci. Total Environ. 267 (2001) 23–31.

[7] K. Pirkanniemi, S. Metsarinne, M. Sillanpaa, Degradation of EDTA and novel complexing agents in pulp

and paper mill process and waste waters by Fenton's reagent, J. Hazard. Mater. 147 (2007) 556–561.

[8] F.G. Kari, W. Giger, Speciation and fate of ethylenedi-aminetetraacetate (EDTA) in municipal wastewater treatment, Water Res. 30 (1996) 122–134.

[9] M. Sillanpää, R. Kokkonen, M.-L. Sihvonen, Determination of EDTA and DTPA as their Fe(III) complexes in pulp and paper mill process and waste waters by liquid chromatography, Anal. Chim. Acta 303 (1995) 187–192.

[10] M. Sillanpää, Comlexing agents in waste water effluents of six finnish pulp and paper mills, Chemosphere 33 (1996) 293–302.

[11] M. Sillanpää, M.-L. Sihvonen, Analysis of EDTA and DTPA, Talanta 44 (1997) 1487–1497.

[12] J. Rämö, M. Sillanpää, V. Vickackaite, M. Orama, L. Niinistö, Chelating ability and solubility of DTPA, EDTA and β-ADA in alkaline hydrogen peroxide environment, J. Pulp. Pap. Sci. 26 (2000) 125–131.

[13] J. Rämö, M. Sillanpää, Degradation of EDTA by hydrogen peroxide in alkaline conditions, J. Cleaner Prod. 9 (2001) 191–195.

[14] M. Sillanpaa, K. Pirkanniemi, Recent developments in chelate degradation, Environ. Technol. 22 (2001) 791–801.

[15] R.D. Ambashta, M. Sillanpää, Experimental design of application of nanoscale iron–nickel under sonication and static magnetic field for mixed waste remediation, J. Hazard. Mater. 189 (2011) 167–172.

[16] W.-X. Zhang, Nanoscale iron particles for environmental remediation: An overview, J. Nanopart. Res. 5 (2003) 323–332.

[17] L. Li, M. Fan, R.C. Brown, J. Van Leeuwen, J. Wang, W. Wang, Y. Song, P. Zhang, Synthesis, properties, and environmental applications of nanoscale iron-based materials: A review, Crit. Rev. Environ. Sci. Technol. 36 (2006) 405–431.

[18] O. Gylienė, T. Vengris, A. Stončius, O. Nivinskienė, Decontamination of solutions containing EDTA using metallic iron, J. Hazard. Mater. 159 (2008) 446–451.

[19] X.-Q. Li, D.W. Elliott, W.-X. Zhang, Zero-valent iron nanoparticles for abatement of environmental pollutants: Materials and engineering aspects, Crit. Rev. Solid State Mater. Sci. 31 (2006) 111–122.

[20] Y.-T. Lin, C.-H. Weng, F.-Y. Chen, Effective removal of AB24 dye by nano/micro-size zero-valent iron, Sep. Purif. Technol. 64 (2008) 26–30.

[21] C. Lee, D.L. Sedlak, Enhanced formation of oxidants from bimetallic nickel−iron nanoparticles in the presence of oxygen, Environ. Sci. Technol. 42 (2008) 8528–8533.

[22] A.D. Bokare, R.C. Chikate, C.V. Rode, K.M. Paknikar, Effect of surface chemistry of Fe−Ni nanoparticles on mechanistic pathways of azo dye degradation, Environ. Sci. Technol. 41 (2007) 7437–7443.

[23] B. Schrick, J.L. Blough, A.D. Jones, T.E. Mallouk, Hydrodechlorination of trichloroethylene to hydrocarbons using bimetallic nickel−iron nanoparticles, Chem. Mater. 14 (2002) 5140–5147.

[24] Y.-H. Tee, E. Grulke, D. Bhattacharyya, Role of Ni/Fe nanoparticle composition on the degradation of trichloroethylene from water, Ind. Eng. Chem. Res. 44 (2005) 7062–7070.

[25] L. Gui, R.W. Gillham, M.S. Odziemkowski, Reduction of N-Nitrosodimethylamine with granular iron and nickel-enhanced iron. 1. Pathways and kinetics, Environ. Sci. Technol. 34 (2000) 3489–3494.

[26] J. Fan, Y. Gao, Nanoparticle-supported catalysts and catalytic reactions—A mini-review, J. Exp. Nanosci. 1 (2006) 457–475.

[27] J. Dong, Z. Xu, S.M. Kuznicki, Magnetic multifunctional nano composites for environmental applications, Adv. Funct. Mater. 19 (2009) 1268–1275.

[28] C. Gomez-Polo, A. Gil, S. Korili, J. Perez-Landazabal, V. Recarte, R. Trujillano, M. Vicente, Magnetic properties of nickel and cobalt catalysts supported on nanoporous oxides, J. Nanosci. Nanotechnol. 8 (2008) 2905–2911.

[29] Z. Zhong, Y. Mastai, Y. Koltypin, Y. Zhao, A. Gedanken, Sonochemical coating of nanosized nickel on alumina submicrospheres and the interaction between the nickel and nickel oxide with the substrate, Chem. Mater. 11 (1999) 2350–2359.

[30] T.V. Reshetenko, L.B. Avdeeva, V.A. Ushakov, E.M. Moroz, A.N. Shmakov, V.V. Kriventsov, D.I. Kochubey, Y.T. Pavlyukhin, A.L. Chuvilin, Z.R. Ismagilov, Coprecipitated iron-containing catalysts (Fe–Al$_2$O$_3$, Fe–Co–Al$_2$O$_3$, Fe–Ni-Al$_2$O$_3$) for methane decomposition at moderate temperatures, Appl. Catal., A 270 (2004) 87–99.

[31] T.V. Reshetenko, L.B. Avdeeva, A.A. Khassin, G.N. Kustova, V.A. Ushakov, E.M. Moroz, A.N. Shmakov, V.V. Kriventsov, D.I. Kochubey, Y.T. Pavlyukhin, A.L. Chuvilin, Z.R. Ismagilov, Coprecipitated iron-containing catalysts (Fe–Al$_2$O$_3$, Fe–Co–Al$_2$O$_3$, Fe–Ni–Al$_2$O$_3$) for methane decomposition at moderate temperatures-I. Genesis of calcined and reduced catalysts, Appl. Catal., A 268 (2004) 127–138.

[32] W. Teunissen, A.A. Bol, J.W. Geus, Magnetic catalyst bodies, Catal. Today 48 (1999) 329–336.

[33] E. Boellaard, A.M. van der Kraan, J.W. Geus, Preparation, reduction, and CO chemisorption properties of a cyanide-derived Fe/Al$_2$O$_3$ catalyst, Appl. Catal., A 147 (1996) 207–227.

[34] M.J. Watts, K.G. Linden, Photooxidation and subsequent biodegradability of recalcitrant tri-alkyl phosphates TCEP and TBP in water, Water Res. 42 (2008) 4949–4954.

[35] D.F. Laine, A. Blumenfeld, I.F. Cheng, Mechanistic study of the ZEA organic pollutant degradation system: Evidence for H$_2$O$_2$, HO•, and the Homogeneous Activation of O$_2$ by Fe^{II} EDTA, Ind. Eng. Chem. Res. 47 (2008) 6502–6508.

[36] C.R. Keenan, D.L. Sedlak, Ligand-enhanced reactive oxidant generation by nanoparticulate zero-valent iron and oxygen, Environ. Sci. Technol. 42 (2008) 6936–6941.

[37] C.E. Noradoun, I.F. Cheng, EDTA degradation induced by oxygen activation in a zerovalent iron/air/water system, Environ. Sci. Technol. 39 (2005) 7158–7163.

[38] T. Zhou, X. Lu, J. Wang, F.-S. Wong, Y. Li, Rapid decolorization and mineralization of simulated textile wastewater in a heterogeneous Fenton like system with/without external energy, J. Hazard. Mater. 165 (2009) 193–199.

[39] D.M. Cwiertny, S.J. Bransfield, A.L. Roberts, Influence of the oxidizing species on the reactivity of iron-based bimetallic reductants, Environ. Sci. Technol. 41 (2007) 3734–3740.

[40] A.D. Bokare, R.C. Chikate, C.V. Rode, K.M. Paknikar, Iron–nickel bimetallic nanoparticles for reductive degradation of azo dye Orange G in aqueous solution, Appl. Catal., B 79 (2008) 270–278.

[41] C. Noubactep, On the operating mode of bimetallic systems for environmental remediation, J. Hazard. Mater. 164 (2009) 394–395.

[42] I. Sanchez, F. Stüber, J. Font, A. Fortuny, A. Fabregat, C. Bengoa, Elimination of phenol and aromatic compounds by zero valent iron and EDTA at low temperature and atmospheric pressure, Chemosphere 68 (2007) 338–344.

[43] X. Du, Y. Wang, X. Su, J. Li, Influences of pH value on the microstructure and phase transformation of aluminum hydroxide, Powder Technol. 192 (2009) 40–46.

[44] J.M. Saniger, N.A. Sánchez, J.O. Flores, Partial fluorination of γ-alumina by gaseous fluorine. J. Fluorine Chem. 88 (1998) 117–125.

[45] K.C. Lanigan, K. Pidsosny, Reflectance FTIR spectroscopic analysis of metal complexation to EDTA and EDDS, Vib. Spectrosc. 45 (2007) 2–9.

[46] B. Liu, R. Hu, J. Deng, Studies on a potentiometric urea biosensor based on an ammonia electrode and urease, immobilized on a γ-aluminum oxide matrix, Anal. Chim. Acta 341 (1997) 161–169.

[47] E.G. Petrov, I.S. Tolokh, V. May, Blocking of bridge-mediated electron transfer by an external magnetic field, Chem. Phys. Lett. 294 (1998) 19–25.

[48] M.J. Watts, K.G. Linden, Advanced oxidation kinetics of aqueous trialkyl phosphate flame retardants and plasticizers, Environ. Sci. Technol. 43 (2009) 2937–2942.

[49] H.F. Aly, Wet-oxidation of spent organic waste tributyl phosphate/diluents, J. Radioanal. Nucl. Chem. 249 (2001) 643–647.

[50] N. Gokulakrishnan, A. Pandurangan, P.K. Sinha, Catalytic wet peroxide oxidation technique for the removal of decontaminating agents ethylenediaminetetraacetic acid and oxalic acid from aqueous solution using efficient Fenton type Fe-MCM-41 mesoporous materials, Ind. Eng. Chem. Res. 48 (2008) 1556–1561.